Thermochimica Acta, 238 (1994) 351–370
Elsevier Science B.V., Amsterdam
SSDI 0040-6031(93)01572-K

High pressure DSC investigations on *n*-alkanes, *n*-alkane mixtures and polyethylene

G.W.H. Höhne * and K. Blankenhorn
Sektion für Kalorimetrie, Universität Ulm, D-89069 Ulm (Germany)

(Received 8 May 1993; accepted 19 October 1993)

Abstract

A high pressure cell for a power-compensated DSC is presented, allowing measurements at pressures up to 500 MPa. With the aid of this apparatus, *n*-alkanes, binary *n*-alkane mixtures, and two linear polyethylenes have been investigated. The fusion temperature and the heat of fusion have been measured for different *n*-alkanes in the pressure region between normal pressure and up to 500 MPa. For five eutectic and non-eutectic binary mixtures, the liquidus and solidus temperatures were determined. It is possible to describe the mixing behaviour of *n*-alkanes with the one-parameter approximation derived by Porter. The increase of the Porter parameter with pressure implies decreasing miscibility at higher pressures. From the Porter parameter the critical point can be calculated. Thus, it can be seen that *n*-alkanes which build mixed crystals at normal pressure demix at higher pressures. From these results, it can be concluded that the same is true for polyethylene.

INTRODUCTION

n-Alkanes have often been considered as model systems that can assist in understanding the structure of polymers of polyethylene type. The multi-lamellar partial crystallization behaviour of polyethylene has led several authors (see, for example, refs. 1 and 2) to describe this material with the help of the thermodynamics of a multi-component *n*-alkane system [3]. It is well known that *n*-alkanes build a lamellar structure in the solid state. The melting point, the heat of fusion and the structure correlate well with the number of carbon atoms in the chain [4, 5] and can be calculated quantitatively from that number [6, 7]. It has been shown that the thermodynamic potential functions depend only on almost unchanged incremental values per CH_2 group and on additional terms due to the end group [8]. Thus it seems promising to try to calculate the mixing behaviour of *n*-alkanes quantitatively and then to transfer the results to polyethylenes. In this way, Kilian and co-workers for example, succeeded in

* Corresponding author.

describing polyethylene wax as a quasi-eutectic system in which the components are mainly chain-folded lamellae organized in spherulites and chain-extended lamellae within and outside the spherulites, respectively [9].

It was found that at normal pressure the superstructure follows the same thermodynamic rules as minor complex systems in which the components are small molecules, e.g. *n*-alkanes. The thermodynamics of mixtures would seem a powerful tool with which to describe the behaviour of these systems. The aim of our investigations was to complement that work by adding another variable, namely the pressure, which is mostly held constant. We first investigated the influence of its variation on the thermodynamic behaviour of *n*-alkane mixtures and polyethylene.

Because there is no high-pressure DSC available on the market, we had to construct one suitable for use up to a hydrostatic pressure of 500 MPa.

EXPERIMENTAL

The high-pressure DSC cell

Because our group already had several power-compensated DSCs (Perkin-Elmer Corp.), we constructed a high-pressure cell that could be plugged into the DSC, instead of the normal double furnace. Thus, we had to use PT-10 resistors as both temperature probe and heater. To avoid difficulties in compatibility, we took these resistors from the original Perkin-Elmer DSC furnaces. We chose silicon oil as the pressure medium because of the very complicated and dangerous handling of high-pressure gas installations. The disadvantages of using a liquid, namely the limited temperature range and the larger heat conductivity, were of minor importance, because the material being investigated was also organic. Thus the temperature range of the high-pressure DSC cell could be limited to 300°C and there were minor difficulties with heat leaks. For the same reason, the furnace could be built of aluminium (with a much better heat conductivity than platinum) with the convection shields being made of glass ceramics. For details of the construction (see ref. 10).

Calibration

There are no temperature and heat calibration materials for high-pressure DSC. The pressure dependence of the fusion temperature of indium has been measured [11, 12], but the results differ depending on the assumptions made concerning the pressure dependence of the resistor thermometer used. The pressure behaviour of the enthalpy of fusion of indium is not known, apart from thermodynamic valuations.

Therefore, we measured both quantities using a high-pressure dilatometer and (for comparison) the new DSC cell [13]. The results can be condensed into the linear equations

$$T_{fus}^{ln}(p) = 429.744 + (0.0473 \pm 0.0005)p$$

$$\Delta h_{fus}^{ln}(p) = 28.62 - (7 \pm 13) \times 10^{-5}p$$

with temperature T in kelvin, specific enthalpy h in J g^{-1}, pressure p in MPa.

The fusion enthalpy is independent of pressure within the limits of accuracy, whereas the fusion temperature changes distinctly, but to a somewhat minor extent, as already known from the literature. With our results, both temperature and heat calibration of the high-pressure DSC are possible.

Sample preparation

Commercially available *n*-alkanes (Humphrey, Ventron and Fluka) of highest possible purity (95%–99% depending on chain length *n*) were used for DSC measurements and preparation of the binary mixtures of different compositions.

The components were weighed directly into the original Perkin-Elmer sample pans, mixed by heating above the melting points, cooled quickly to room temperature and hermetically sealed. Care was taken to avoid inclusion of bubbles or cavities, which can cause severe deformation and leaking of the pans under pressure. The sample masses used were 1 to 10 mg, and the heating rates were 0.5 to 10 K min^{-1}. Small masses and low heating rates are preferable in order to avoid peak falsification (smearing) as a result of thermal relaxation processes. However, this leads to a bad signal-to-noise ratio and thus restricts the accuracy of the evaluation. An approximate compromise had to be found for each individual case.

The samples of high-density polyethylene (Lupolen 6011, $M_w = 120{,}000$, $M_w/M_n = 3.43$; number of side CH_3 groups per 1000 C-atoms < 1) and polyethylene wax (PE130, $M_w = 4650$, $M_w/M_n = 3.63$; number of side CH_3 groups per 1000 C-atoms < 1) were prepared in a similar manner.

Evaluation

The high-pressure DSC experiments yielded measuring curves that are typical of those from common power-compensated DSCs (Fig. 1). In general, a baseline run (with empty pans) was recorded and subtracted from the sample run. The evaluation led, as usual, to extrapolated onset temperatures and peak areas, from which the beginning of the transition process and the heat of transition could be determined with the aid of the calibration results.

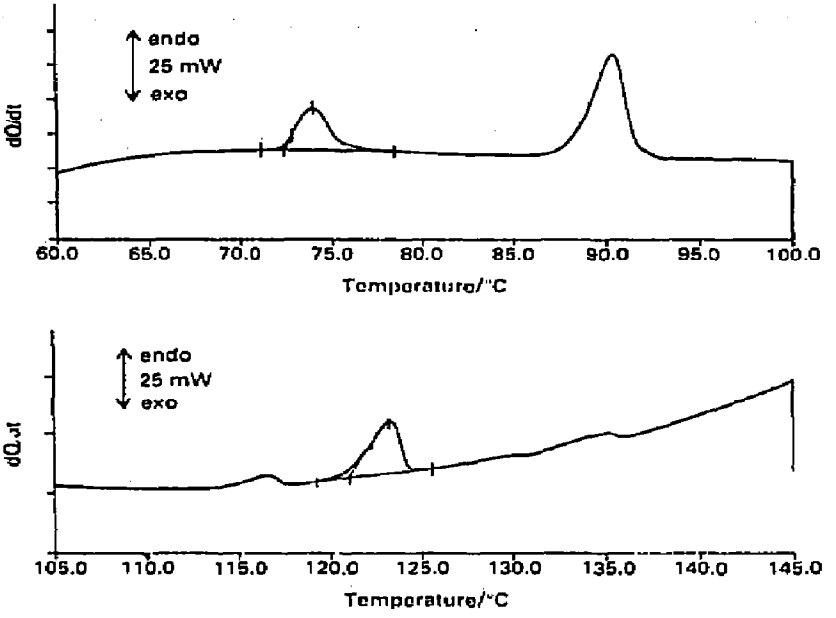

Fig. 1. Typical original measured curves from high pressure DSC. Upper curve: C_{28}/C_{24} mixture with solid solubility at 150 MPa (mass, 4.4 mg; heating rate, 10 K min^{-1}). Lower curve: eutectic C_{32}/C_{24} mixture at 400 MPa (mass, 3.75 mg; heating rate, 5 K min^{-1}).

With binary mixtures and polyethylene, the end of the temperature region of the fusion process must also be known, because it characterizes the liquidus curve of the phase diagram. This temperature is not easy to determine. The extrapolated peak end temperature is systematically too large, because of thermal relaxation processes in the DSC and also in the sample. The magnitude of the necessary correction depends on sample mass, heating rate and the quality of the thermal contact, and must be determined separately in a series of experiments. Theoretical considerations [14] have provided a formula for determining the true end of the fusion process from the shape of the measured peak, i.e. at the end of the linear part of the increasing flank of the peak. But this method only holds in special cases (e.g. eutectic fusion) and, because of its systematic uncertainty, yields no better results than the empirical method.

The evaluation described was usually made on heating runs. Cooling runs were also carried out, but a precise evaluation is generally not possible here, because of undefined undercooling phenomena.

EXPERIMENTAL RESULTS

Pure n-*alkanes*

The transition temperatures of eight *n*-alkanes were measured at different pressures up to 500 MPa. The results agree with earlier measurements [15–17]. Table 1 and Fig. 2 illustrate the dependence of the fusion

TABLE 1

Pressure dependence of the fusion temperatures (in K) of different *n*-alkanes and of the extrapolated fusion temperature of an infinite chain

Pressure/MPa	C_{24}	C_{26}	C_{28}	C_{30}	C_{32}	C_{38}	C_{44}	C_{60}	T^{∞}_{fus}
0.1	323.8	329.5	334.4	338.6	342.5	352.2	359.6	372.4	415.0
50	335.6	340.8	346.7	351.8	354.1	365.8	371.5	386.2	428.1
100	346.4	352.1	357.9	362.7	365.3	376.7	383.7	397.9	440.5
200	367.3	372.6	378.0	382.5	386.1	396.7	403.2	419.4	460.2
300	384.8	389.4	395.2	400.2	403.8	414.4	420.0		477.3
350		397.2	402.8	408.9		421.9	429.4	446.1	
400	401.1				420.0		436.0	452.1	491.4
500	416.3				436.2			467.5	507.9

temperature on pressure. The measured values can be fitted with second-order polynomials; the average curve reads

$$T_{fus} = T_{fus}(p = 0.1) + (0.2451 \pm 0.009)p - (1.33 \pm 0.2) \times 10^{-4}p^2 \quad (1)$$

where T is in K or °C and p is in MPa.

The fusion temperature of *n*-alkanes at normal pressure can be calculated from the number of carbon atoms in the chain as follows (data from ref. 4)

$$\frac{1}{T_{fus}} = (16.48 \pm 0.01) \times 10^{-4}n^{-1} + (2.4096 \pm 0.0015) \quad (2)$$

where T is in K and n is the number of carbon atoms.

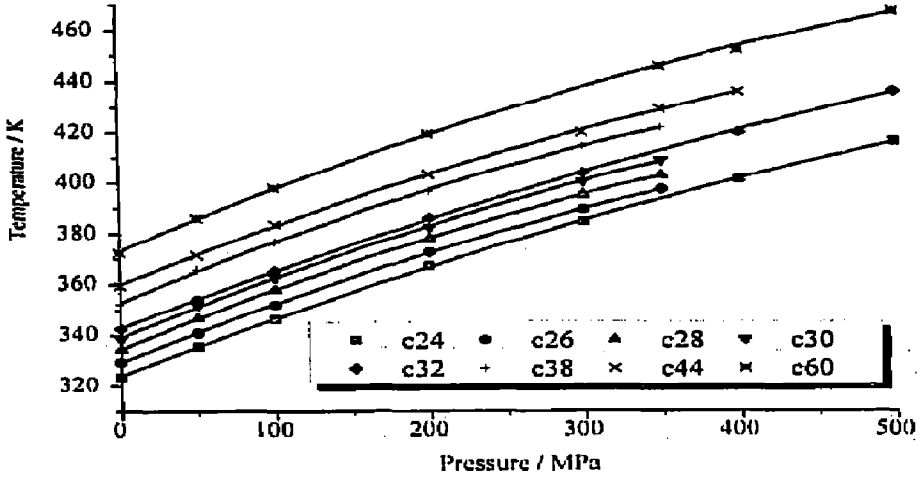

Fig. 2. Pressure dependence of fusion temperatures of *n*-alkanes. Points are measured values corrected for zero heating rate; solid lines are calculated parabolic least-squares fits.

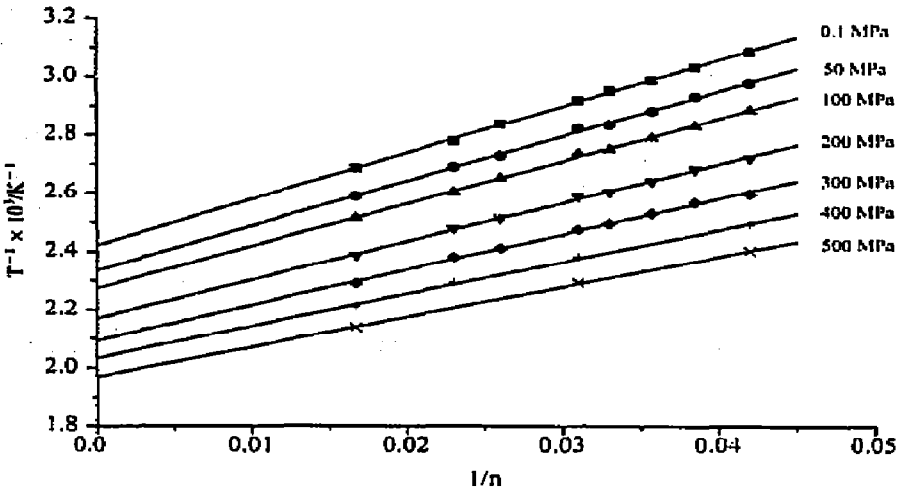

Fig. 3. Dependence of fusion temperatures on numbers of carbon atoms. Points are measured values corrected for zero heating rate; solid lines are calculated least-squares fits.

In other words, the reciprocal fusion temperature depends on the reciprocal number of carbon atoms in a linear manner. As can be seen from Fig. 3, the same is true for larger pressures, but the slope of the straight line in question decreases with increasing pressure. From these fit lines the fusion temperature of the infinite *n*-alkane chain (see Table 1) and its pressure dependence can be obtained by extrapolation

$$T^{\infty}_{fus}(p) = 414.8 + 0.2503p - 1.348 \times 10^{-4}p^2 \quad (3)$$

with T in K and p in MPa. This function is only slightly steeper than that of *n*-alkanes with n ranging from 24 to 60 (eqn. (1)).

A figure similar to Fig. 2 can also be plotted for the solid–solid transition (Table 2) of the lower *n*-alkanes. The slopes of these curves are larger. Thus the distance between the transition and fusion peak (which can easily be resolved at low heating rates both in the normal and in the high-pressure

TABLE 2

Pressure dependence of the transition temperatures (K) and triple points of different *n*-alkanes

Pressure/MPa	C_{24}	C_{26}	C_{28}	C_{30}	C_{32}	C_{38}
0.1	321.4	325.8	330.7	334.8	338.2	349.5
25	327.5	332.4	–	342.8	344.8	357.1
50	334.9	338.6	–	350.6	351.3	364.6
100	–	–	–	–	363.8	376.7
Triple point/MPa	70–75	120–130		70–80	110–120	180–190

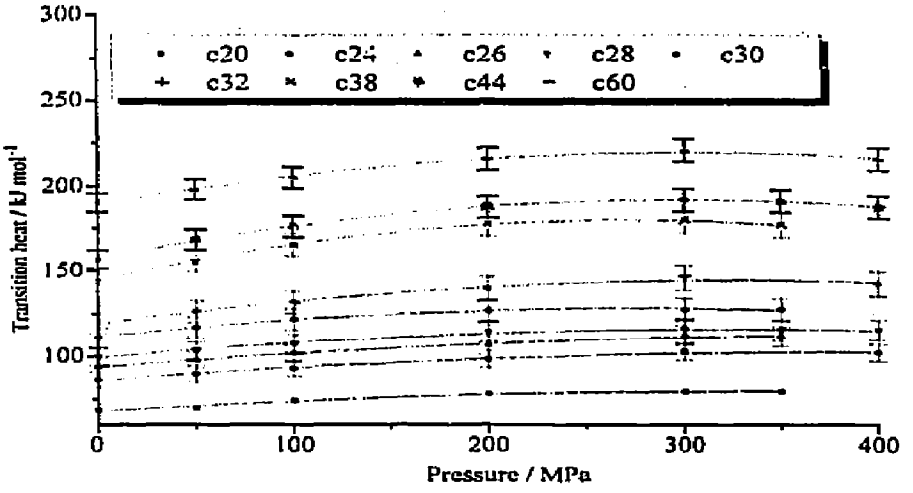

Fig. 4. Pressure dependence of the total heat of transition and fusion of *n*-alkanes. Points are averaged measured values; solid lines are calculated parabolic least-squares fits.

cell of the DSC, see Fig. 1) decreases with increasing pressure, and the former ceases at the triple point in the region of 100–200 MPa, in accordance with the results of Koppitz and Würflinger [16].

The pressure dependence of the total heat of transition (solid–solid and fusion) is represented in Fig. 4. There is only a slight increase of 10% up to 300 MPa; then the heat of transition seems to decrease again. Similar results were found by Dollhopf [17] using high pressure dilatometry, also for shorter *n*-alkanes.

Binary mixtures

Two eutectic *n*-alkane binary mixtures and three non-eutectic mixtures have been investigated in the high-pressure DSC. The measured heat curves (Table 3) yielded mainly phase diagrams, two examples of which, one eutectic and one with solid miscibility, are presented in Figs. 5–8.

The determined heats of transition, within the limits of accuracy were equal to those calculated from the pure components, corresponding to the composition of the mixture. The pressure dependence of the transition heats did not differ significantly from that for the pure *n*-alkanes.

Polyethylene

A rather complex fusion behaviour was found for high-density polyethylene (HDPE), in agreement with the results of other authors [18, 19]. Figure 9 shows the change in shape of the fusion (and transition) peak of HPDE with pressure. In this figure, the temperature axes for each pressure have been shifted relative to the temperature of the infinite chain obtained

TABLE 3

Measured temperatures (in K) of the beginning (solidus, T^s) and end (liquidus, T^l) of transitions for different binary mixtures of *n*-alkanes. All temperatures have been corrected for zero heating rate

Volume fraction	0.1 MPa		50 MPa		100 MPa		150 MPa		200 MPa		250 MPa		300 MPa		350 MPa		400 MPa		500 MPa		550 MPa	
	T^s	T^l	T^s	T^l	T^s	T^l	T^s	T^l	T^s	T^l	T^s	T^l	T^s	T^l	T^s	T^l	T^s	T^l	T^s	T^l	T^s	T^l
C_{32}/C_{24} (eutectic)																						
0.19	323.4	324.3																				
0.31	323.4	328.5																				
0.34	323.5	329.0	336.1	342.0	346.0	353.0			363.4	374.2			379.6	391.8			394.2	408.5	408.2	423.8		
0.35	323.4	329.1																				
0.44	323.3	332.6	335.3	343.9	345.0	355.5			363.7	375.8			380.0	393.7			393.8	410.4	408.2	425.9		
0.47	323.4	333.1	336.1	344.3	345.8	355.6			363.4	376.5			379.5	394.5			394.8	410.7	408.6	426.7		
0.52	323.4	334.1																				
0.53	323.4	334.1	335.8	346.0	345.2	357.4			364.1	379.0			379.8	396.8								
0.57	323.4	335.3																				
0.65	323.4	336.4																				
0.75	323.4	338.5																				
0.86	323.4	340.0																				

C_{60}/C_{44} (eutectic)																		
0.18	359.1	360.2																
0.32	359.5	364.3																
0.36	359.2	365.0																
0.37	359.3	364.7																
0.41	359.6	365.8	370.3	379.6	381.6	391.3			400.9	412.9			419.1	430.7				
0.43	358.9	366.4	370.0	380.1	381.9	392.3			401.4	413.6			418.9	431.4			435.3	446.4
0.50	359.2	367.1																
0.51	359.4	367.3																
0.53	359.2	367.8	370.4	381.8	382.6	393.5			401.4	418.8			419.3	432.6			435.6	447.6
0.57	359.6	368.0																
C_{28}/C_{24}																		
0.33	325.0	327.8																
0.36	325.0	327.8									376.0	378.9	382.9	385.6	390.8	392.3	398.1	400.1
0.39	325.7	327.9	337.9	340.5	349.0	351.8	359.0	361.5	367.7	370.3	376.2	379.1	383.1	385.9	390.6	392.6	397.8	400.2
0.47	325.8	328.8																
0.52	326.5	329.3																
C_{32}/C_{26}																		
0.39	329.2	332.9	340.4	344.1	351.3	355.0	362.3	365.0	371.3	375.0	379.6	383.5	387.4	391.9	394.7	399.0		
0.54	330.2	335.9																
0.75	333.1	338.3																
C^{30}/C^{24}																		
0.22	324.0	325.8																
0.45	324.2	327.8																
0.6	325.3	330.5	337.1	344.0	347.6	355.9			366.8	375.3	375.0	384.1		389.8	401.0	398.3	409.2	

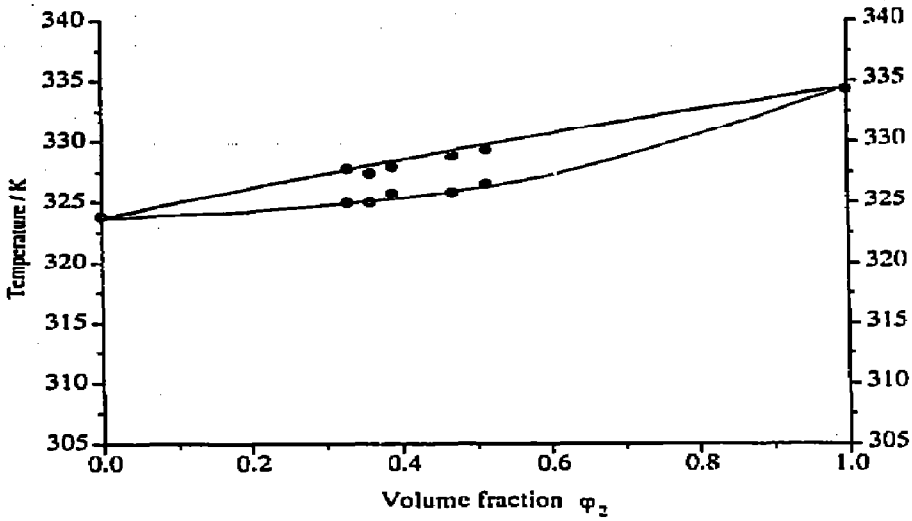

Fig. 5. Phase diagram of C_{28}/C_{24} mixture at normal pressure. Points are measured values with masses of 2.5–4.5 mg and heating rates of 5–10 K min^{-1}; solid lines are calculated values.

from eqn. (3). Thus the overlapping temperatures, are equivalent relative to the fusion behaviour of long chain *n*-alkanes. At pressures above 300 MPa the peak splits into two, where the first peak characterizes the transition into the hexagonal phase (the so-called 'condis phase' [20]) and the second represents the fusion peak. (An additional low temperature peak also appears, see the discussion on PE wax.) In Fig. 10, the end-of-fusion temperatures and the transition temperatures are plotted as a function of pressure. The curve undergoes a parallel shift in the region of

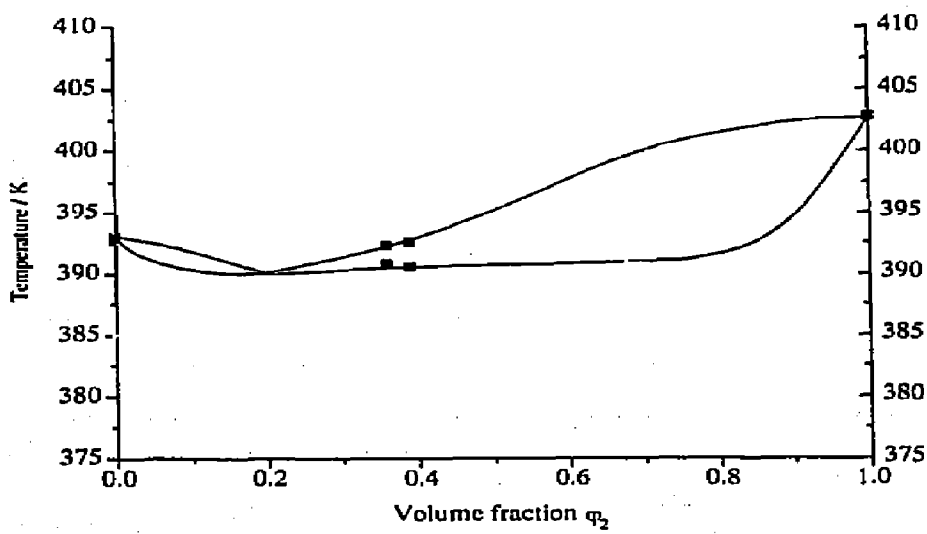

Fig. 6. Phase diagram of C_{28}/C_{24} mixture at 350 MPa pressure. Points are measured values with masses of 4–5 mg and heating rate 10 K min^{-1}; solid lines are calculated values.

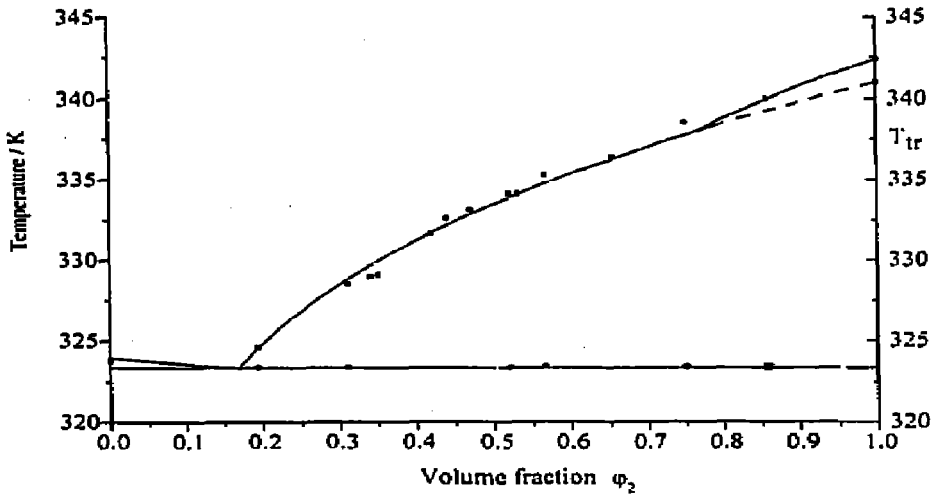

Fig. 7. Phase diagram of C_{32}/C_{24} mixture at normal pressure. Points (●, ■) are measured values with mass of 1.5–10 mg and heating rates of 0.5–10 K min^{-1}; solid lines are calculated values.

200 to 300 MPa. We assume that this is caused by the change from folded- to extended-chain crystals with a corresponding change in fusion temperature.

Figures 11 and 12 show similar curves for polyethylene wax. In this case no transition into a condis phase could be found. But at increasing pressure another small peak seems to develop on the lower temperature side of the fusion peak. This small peak suggests phase separation phenomena (possibly carried by molar mass induced segregation) rather than a solid–solid transition as in HDPE.

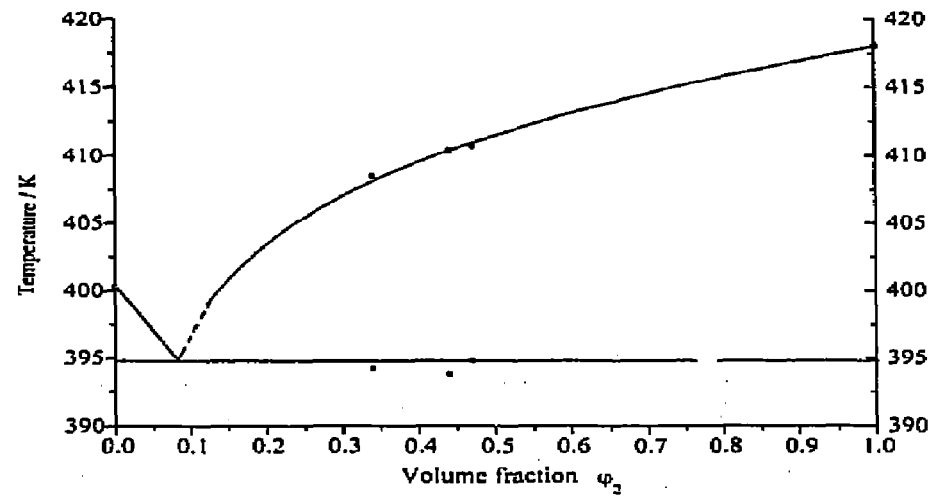

Fig. 8. Phase diagram of C_{32}/C_{24} mixture at 400 MPa pressure. Points (●, ■) are measured values with masses of 2–5 mg and heating rate 10 K min^{-1}; solid lines are calculated values.

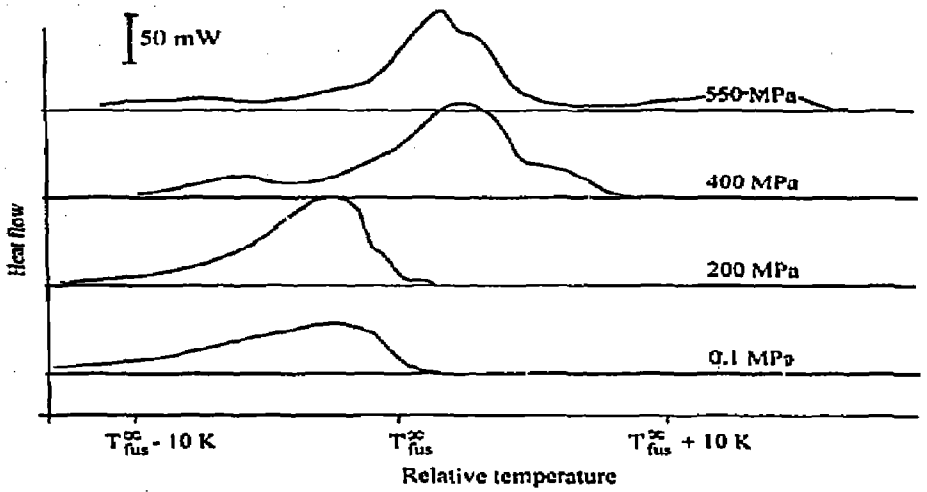

Fig. 9. DSC endotherm curves of HDPE at different pressures (mass, 11 mg; heating rate, 10 K min^{-1}). The temperature has been shifted for the different pressures corresponding to eqn. (3).

DETERMINATION OF EXCESS THERMODYNAMIC POTENTIAL FUNCTIONS

Thermodynamics gives the theoretical background for the calculation of the liquidus and solidus curves of phase diagrams [21]. In the case of ideal binary mixtures the formula reads

$$\ln x_i^l - \ln x_i^s = \int_{T_i}^{T} \frac{\Delta H_i^*}{RT^2} \mathrm{d}T \tag{4}$$

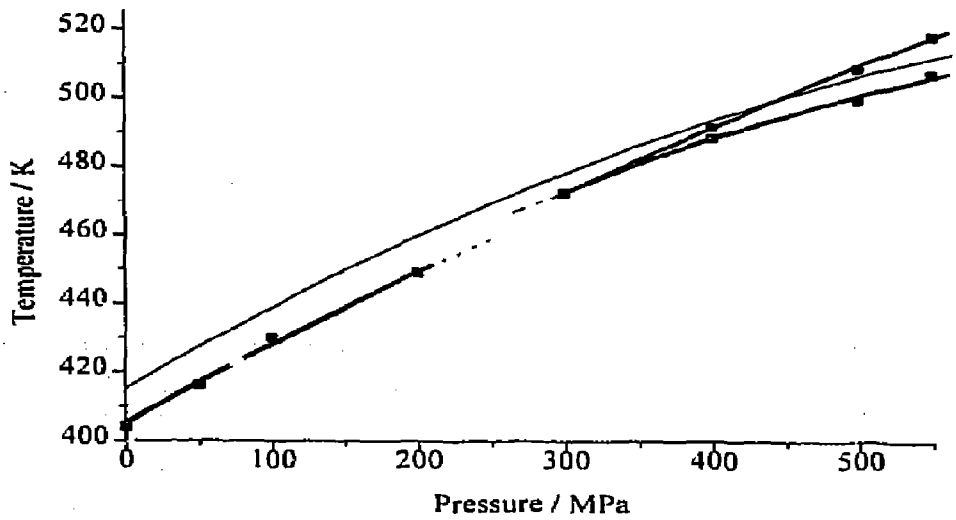

Fig. 10. Pressure dependence of the corrected maximal fusion temperature for HDPE. At higher pressures, there is an additional transition into hexagonal phase. The thin line marks the fusion temperature of the infinite chain. Points are measured values.

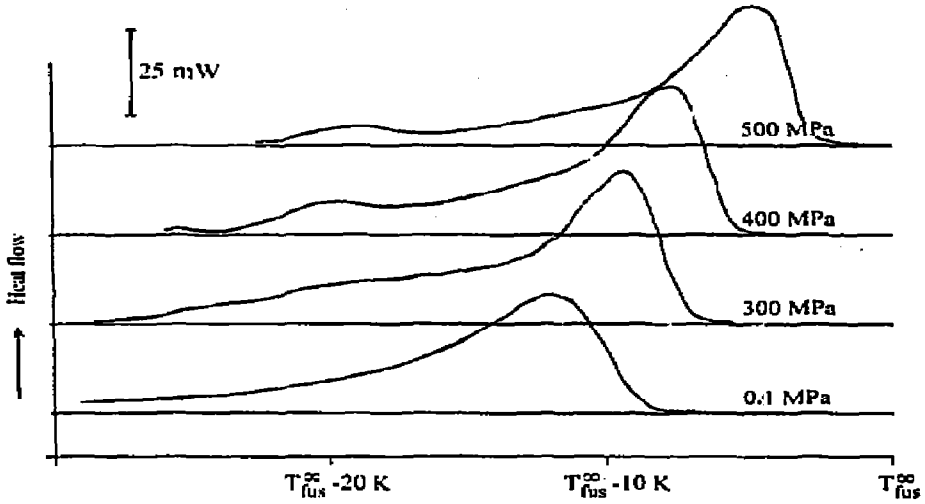

Fig. 11. DSC enotherm curves of PE 130 at different pressures (mass, 11 mg; heating rate, 10 K min $^{-1}$). The temperature has been shifted for the different pressures corresponding to eqn. (3).

where i is 1 or 2, l is liquidus, s is solidus, x mole fraction, ΔH_i^* transition enthalpy of pure component i, T temperature, and T_i transition temperature of pure component i.

In the case of non-ideal mixtures, we have to exchange the mole fraction x with the activity a. The activity is expressed

$$a = xf$$

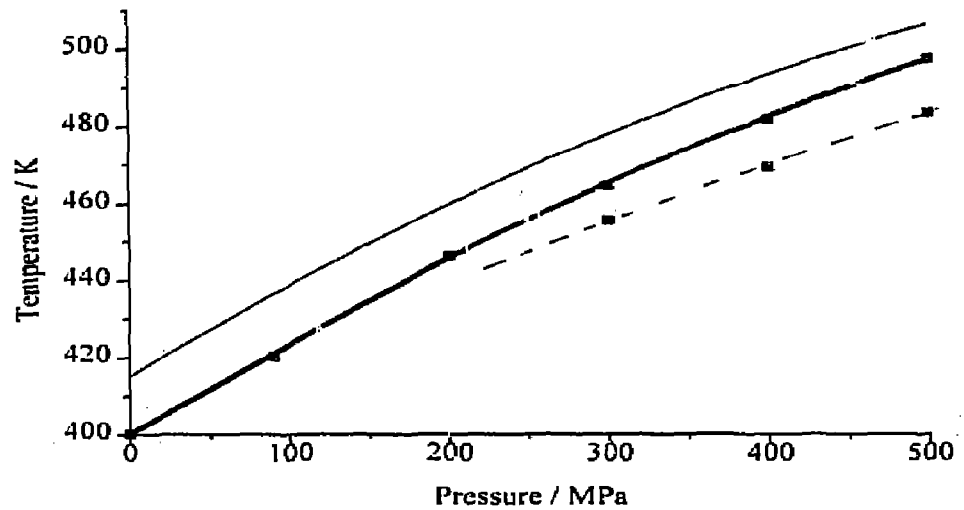

Fig. 12. Pressure dependence of the corrected maximal fusion temperature for PE 130. The thin line marks the fusion temperature of the infinite chain. The broken line marks an additional peak. Points are measured values.

where f is the activity coefficient. Substituting this into eqn. (4)

$$\ln(x_i^l f_i^l) - \ln(x_i^s f_i^s) = \int_{T_i}^{T} \frac{\Delta H_i^*}{RT^2}\,dT \tag{5}$$

The activity coefficient can be expressed in a different manner. The easiest is as described by Porter [22], with only one parameter. This usually holds for non-electrolyte solutions, as is the case for n-alkane mixtures

$$RT \ln f_1 = A(p, T)x_2^2$$

and

$$RT \ln f_2 = A(p, T)x_1^2 \tag{6}$$

The so-called Porter parameter A is usually different for the liquid (l) and solid (s) solutions, and also depends on pressure and temperature. Inserting eqn. (6) into eqn. (5) yields a system of two implicit coupled equations, which must be solved to obtain the liquidus $T(x^l)$ and solidus $T(x^s)$ curves. Normally this can only be done iteratively with the aid of a computer. In the case of n-alkanes, eqn. (5) simplifies because the enthalpies of transition and fusion do not depend significantly on temperature and can, therefore, be inserted in front of the integral, yielding the equation system

$$\ln x_1^l + \frac{A^l}{RT}(x_2^l)^2 - \ln x_1^s - \frac{A^s}{RT}(x_2^s)^2 = \frac{\Delta H_1^*}{R}\left(\frac{1}{T_1} - \frac{1}{T}\right) \tag{7a}$$

$$\ln x_2^l + \frac{A^l}{RT}(x_1^l)^2 - \ln x_2^s - \frac{A^s}{RT}(x_1^s)^2 = \frac{\Delta H_2^*}{R}\left(\frac{1}{T_2} - \frac{1}{T}\right) \tag{7b}$$

In the case of eutectic systems (with no miscibility in the solid phase), the activity coefficients in the solid phase f^s are equal to unity, and the third and fourth terms of the left side of eqns. (7a) and (7b) disappear.

From thermodynamics, it follows that the excess free enthalpy can be expressed

$$G^E = x_1 RT \ln f_1 + x_2 RT \ln f_2$$

Inserting eqn. (6) gives

$$G^E = Ax_1x_2 \tag{8}$$

This is a parabolic function with a maximum at $x_i = 0.5$. The same is true for the other excess functions

$$S^E = -\left|\frac{\partial A}{\partial T}\right|_p x_1x_2 \tag{8a}$$

$$V^E = \left|\frac{\partial A}{\partial p}\right|_T x_1x_2 \tag{8b}$$

$$H^E = \left(A - \left|\frac{\partial A}{\partial T}\right|_p T\right)x_1x_2 \tag{8c}$$

Measurements have shown [23, 24] that the excess functions are slightly asymmetric relative to the mole fraction, but become more symmetric if we replace the mole fraction by the volume fraction. This is also a result of the principle of congruence [25]. The volume fraction is defined as

$$\varphi_i = \frac{r_i n_i}{r_1 n_1 + r_2 n_2} \tag{9}$$

where r_i the number of volume elements in the molecule i, and n_i is the number of moles in the mixture. In the case of n-alkanes, one C_2H_4-group has the same volume as one CH_3-group; this we can calculate r_i from the number of C-atoms n in an n-alkane

$$r_i = \frac{n-2}{2} + 2$$

Huggins [26] has had the same idea for polymer solutions, but he takes r_i as the number of C-atoms of molecule i. The difference in the exact volume fraction is only relevant for smaller molecules. However, in terms of the volume fraction, eqn. (8) reads

$$G^E = A(p, T)\varphi_1\varphi_2 \tag{10}$$

but with a different A parameter. Equations (8a)–(8c) read correspondingly.

Using eqn. (10), the following formulae can be deduced

$$RT \ln f_1 = G^E - x_2 \frac{\partial G^E}{\partial x_1} = A\varphi_2^2[1 + (1 - r_1/r_2)(1 - 2\varphi_2)]$$

$$RT \ln f_2 = G^E - x_1 \frac{\partial G^E}{\partial x_2} = A\varphi_1^2[1 + (1 - r_2/r_1)(1 + 2\varphi)]$$

These equations must be inserted into eqn. (5) together with the definition of the volume fraction φ and the mole fraction x, to obtain a set of equations similar to eqns. (7) but with the other definition of the Porter parameter A.

Thus, we have to fit the measured phase diagrams of the binary mixtures at different pressures by the liquidus and solidus curves calculated from this equation system. The fit parameters are A^l for the liquidus and A^s for the solidus curve. The results of these calculations are shown in Table 4. The Porter parameter is plotted in Figs. 13–15, and, together with other results, in Figs. 16 and 17. In every case the Porter parameter increases with pressure. The calculated liquidus and solidus curves fit the measurements rather well (see Figs. 5–8). It should be added that, for the mixtures with solid solubility, the calculation of the pressure dependence of the A parameters must be considered to be very approximate, because too few measurements have been made.

TABLE 4

Pressure dependence of fit parameter A of different n-alkane mixtures

Pressure/MPa	C_{28}/C_{28}		C_{26}/C_{32}		C_{24}/C_{30}			C_{24}/C_{32}	C_{44}/C_{60}
	$A^{\wedge}$	A^{l}	$A^{\wedge}$	A^{l}	$A^{\wedge}$	A^{l}	A^{sol}	A^{l}	A^{l}
0.1	2100	900	1900	−2500	1900	−3100		−200	−800
50	2100	1000	2400	−2500	2000	−3200		300	−200
100	2100	1000	3200	−2500	2200	−3000		700	300
150	2500	1000	3700	−2500					
200	4100	1000	4100	−2500	4500	−1500	−400	1400	1200
250	4400	1300	4500	−2500	6000	0	800		
300	5700	1300	5400	−2500				1900	2100
350	6500	1300	6500	−2500			3500		
400							4100	2600	2700
500								2900	

Now the question arises: how does A depend on temperature and pressure. By assuming that the excess enthalpy is linearly related to pressure p and temperature T, and the excess volume is linearly related to temperature only, we have applied the following formulation for $A(p, T)$, as derived by Herzfeld and Heitler (see ref. 21)

$$A = a_0 + b_0 p - a_1 T + b_1 pT - a_2 T \ln T \tag{11}$$

To determine these parameters, more information is required. First the heat of mixing for the system C_{32}/C_{24} was measured in a mixing calorimeter (LKB 8700) and the excess enthalpy at normal pressure and 345 K was calculated as 17 J mol^{-1} (at a volume fraction of 0.5). Then the excess

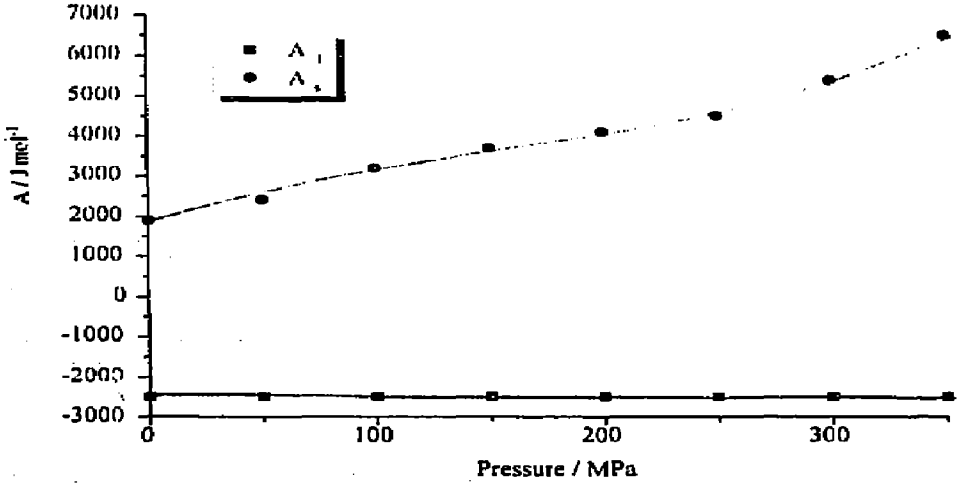

Fig. 13. Pressure dependence of the Porter parameters of C_{32}/C_{26} mixtures. Points (■, ●) mark calculated values for the best fit of liquids and solidus curves.

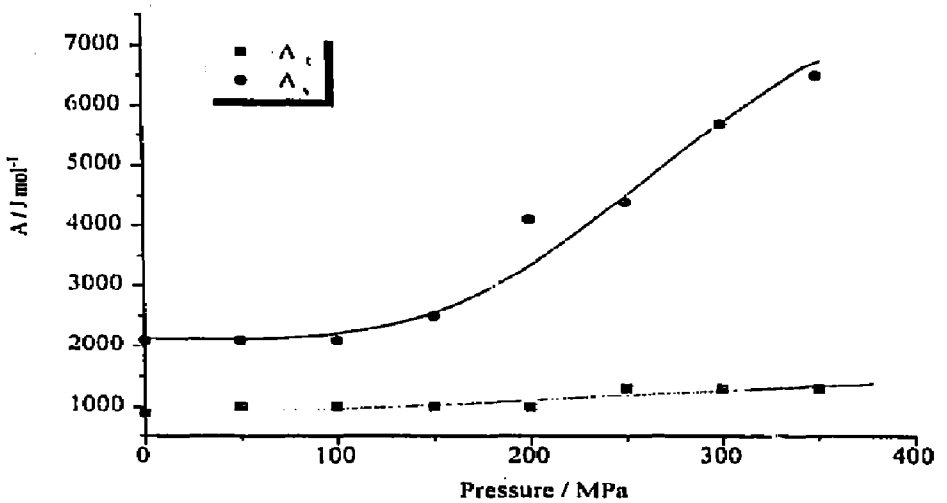

Fig. 14. Pressure dependence of Porter parameters of C_{28}/C_{24} mixtures. Points (■, ●) mark calculated values for the best fit of liquidus and solidus curves.

volume of that mixture under the same conditions was calculated using a formula deduced by Hollemann [27] as 0.018 $cm^3\ mol^{-1}$. Starting from these values, we tried to fit the parameters a_i and b_i of eqn. (11) so that the calculated value of A matches the measured values (Table 4). This was not possible. Instead we had to expand eqn. (11) by adding another pressure term

$$A = a_0 + b_0 p - a_1 T + b_1 pT - a_2 T \ln T + b_2 p \exp(-p/b_3) \quad (12)$$

which was successful.

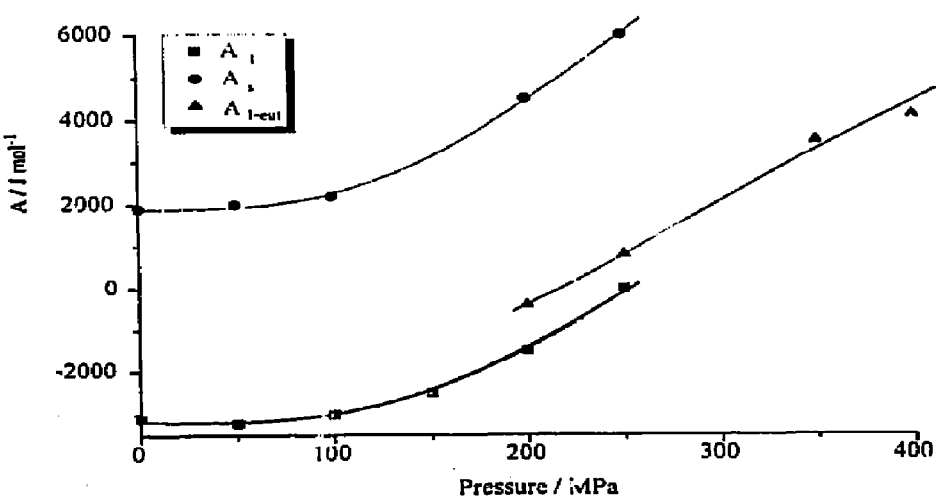

Fig. 15. Pressure dependence of Porter parameters of C_{30}/C_{24} mixtures. Points (■, ●) mark calculated values for the best fit of liquidus and solidus curves; ▲, calculated with eutectic formula.

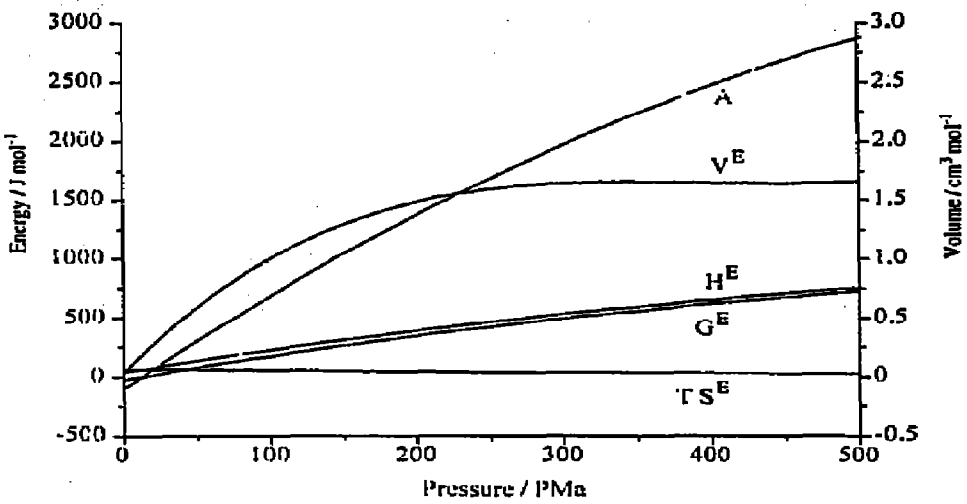

Fig. 16. Pressure dependence of Porter parameter and excess potential functions of C_{32}/C_{24} mixture calculated with eqn. (12).

Using eqns. (8a)–(8c) and (10)

$$\Delta H^{E} = (a_0 + b_0 p + a_2 T + b_2 p \exp(-p/b_3))\varphi_1\varphi_2 \quad (12a)$$

$$\Delta V^{E} = (b_0 + b_1 T + b_2(1 - p/b_3)\exp(-p/b_2))\varphi_1\varphi_2 \quad (12b)$$

$$\Delta S^{E} = (a_1 + a_2 - b_1 p + a_2 \ln T)\varphi_1\varphi_2 \quad (12c)$$

From this expansion it was possible to calculate the measured pressure dependence of the Porter parameter using the set of parameters: $a_0 = 1404$, $a_1 = 28$, $a_2 = -4$, $b_0 = 6.24$, $b_1 = 9.81 \times 10^{-4}$, $b_2 = 6.012$, $b_3 = 200$. The curves in question can be seen in Fig. 16. The same process was applied to the mixture C_{44}/C_{60}; the result is plotted in Fig. 17.

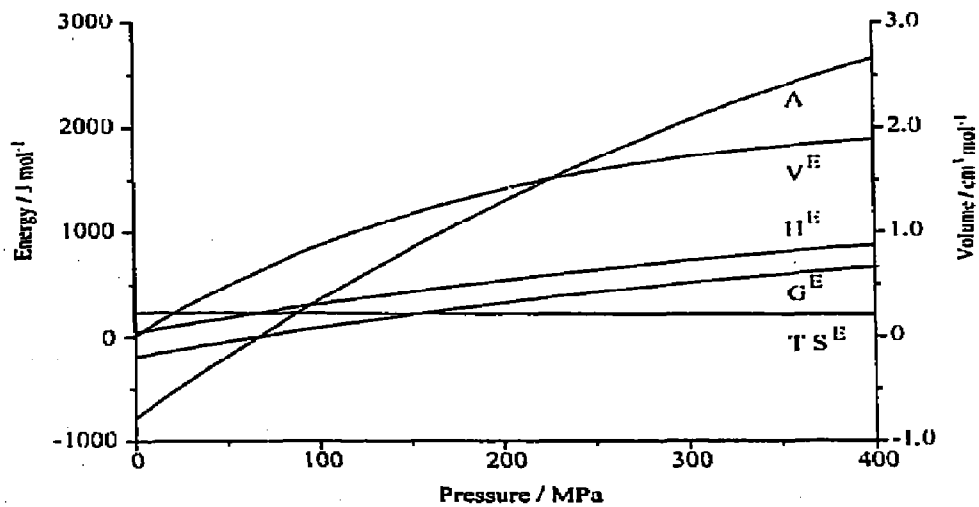

Fig. 17. Pressure dependence of Porter parameter and excess potential functions of C_{60}/C_{44} mixture calculated with eqn. (12).

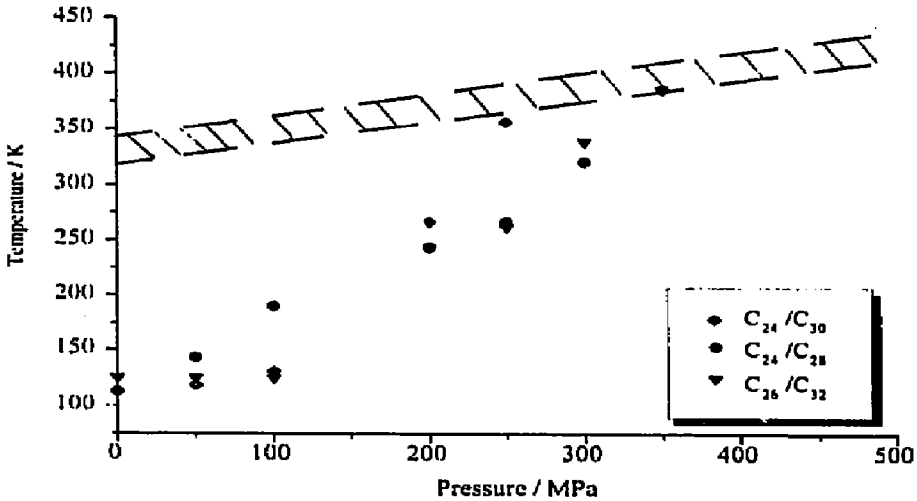

Fig. 18. Pressure dependence of calculated critical temperatures of different mixtures. The hatched area represents the transition and fusion region of the mixtures.

Knowing the Porter parameter, the critical temperature of demixing (and thus the binodal and the spinodal) can be calculated using the formula [21]

$$T^K = A^K/2R$$

The results are shown in Fig. 18. When the critical temperature reaches the region of transition, the homogeneous phase in question becomes unstable and may separate into two. For some solid solutions of the measured binary mixtures, this occurs within the investigated pressure region. For the liquid solution, it can be extrapolated that the phase separation occurs at pressures above the limit of our apparatus.

CONCLUSIONS

It is possible to describe the mixing behaviour of *n*-alkanes with the one-parameter approximation of Porter. The increase in the Porter parameter with pressure implies decreasing miscibility at higher pressures. From the Porter parameter, the critical point can be calculated. Thus it can be seen that *n*-alkanes which build mixed crystals at normal pressure demix at higher pressures. From our results, it can be concluded that the same is true for polyethylene. High-pressure-crystallized polyethylene is in a metastable state at normal pressure, because the crystallization takes place in another miscibility regime, i.e. the A parameter is different.

ACKNOWLEDGEMENT

The authors thank the Deutsche Forschungsgemeinschaft for supporting this project within the SFB 239.

REFERENCES

1 W. Glenz, H.G. Kilian, D. Klattenhoff and F. Stracke, Polymer, 18 (1977) 685.
2 B. Wunderlich and G. Czornyj, Macromolecules, 10(5) (1977) 906.
3 G.I. Asbach and H.G. Kilian, Polymer, 32(32) (1991) 3006.
4 M.G. Broadhurst, J. Res. Natl. Bur. Stand. USA, Sect. A, 66(3) (1962) 241.
5 H.G. Kilian, Progr. Colloid Polym. Sci., 72 (1986) 60.
6 P.J. Flory and A. Vrij, J. Am. Chem. Soc., 85 (1963) 3548.
7 A. Thomson, Philos. Mag., 42 (1871) 484.
8 C.M.L. Atkinson and M.J. Richardson, Trans. Faraday Soc., 65 (1969) 1749.
9 M. Sawodny, G.I. Asbach and H.G. Kilian, Polymer, 31 (1990) 1859.
10 K. Blankenhorn and G.W.H. Höhne, Thermochim. Acta, 187 (1991) 219.
11 R. Sandrock, Dissertation, Universität Bochum, 1982.
12 P.W. Richter and J.B. Clark, Rev. Sci. Instrum., 51 (1980) 559.
13 W. Dollhopf and G.W.H. Höhne, in preparation.
14 J. Schawe, Thermochim. Acta, 229 (1993) 69.
15 M. Kamphausen, Dissertation, Universität Bochum, 1976.
16 B. Koppitz and A. Würflinger, Colloid Polym. Sci., 252 (1974) 999.
17 W. Dollhopf, Dissertation, Universität Ulm, 1979.
18 M. Yasuniwa, Polym. J., 4(5) (1973) 526.
19 D.C. Bassett, Polymer, 17 (1976) 460.
20 B. Wunderlich, M. Möller, J. Grebowicz and H. Baur, Conformational Motion and Disorder in Low and High Molecular Mass Crystals, Springer Verlag, Berlin, 1988.
21 R. Haase, Thermodynamik der Mischphasen, Springer Verlag, Berlin, 1956.
22 A.W. Porter, Trans. Faraday Soc., 16 (1920) 336.
23 J.H. van der Waals and J.J. Hermans, Rec. Trav. Chim. Pays-Bas, 69 (1950) 949, 971.
24 J. Hijmans and Th. Hollemann, Adv. Chem. Phys., 16 (1969) 223.
25 S.P. Koh and A.G. Williamson, Chem. Eng. J., 19 (1980) 85.
26 M.L. Huggins, J. Am. Chem. Soc., 64 (1942) 1712.
27 Th. Holleman, Physica, 29 (1963) 585.